energies

MDPI

Article

Design Aspects and Performance Evaluation of Pole-Phase Changing Induction Machines

Konstantina Bitsi [1,*], Sjoerd G. Bosga [1,2] and Oskar Wallmark [1,†]

[1] Division of Electric Power and Energy Systems, KTH Royal Institute of Technology, 100 44 Stockholm, Sweden
[2] ABB Corporate Research, 722 26 Västerås, Sweden
* Correspondence: bitsi@kth.se
† Deceased.

Abstract: Pole-phase changing induction machines (IMs) offer the capability to extend the torque-speed envelope compared to their fixed pole-phase counterparts. Dynamic pole-changing can achieve higher torque levels at lower speeds, utilizing higher pole numbers, and extended flux-weakening range with lower pole-number operations. This paper investigates the design impact on the optimum pole-phase changing behavior and respective split of the operating region to different pole-phase operations. Additionally, the improvement in terms of the overall torque per ampere capability and efficiency is illustrated. For the purposes of the analysis, two different IMs with wound independently-controlled stator coils (WICSC) and different original pole numbers are evaluated in an effort to quantify the extent of the benefits of pole-phase changing. These geometries correspond to machines that were originally designed with 2- and 6 magnetic poles, respectively. It is shown that, in the case of the original 2-pole WICSC machine, shifting to a higher pole number is notably beneficial in terms of efficiency in a significant part of the operating region, whereas in the original 6-pole, both higher and lower pole numbers significantly enhance the overall torque capability and efficiency. The results highlight the notable benefits of pole-phase changing IMs and offer deep insight towards the derivation of standard design guidelines for these machines.

Keywords: FEM modeling; independently-controlled stator coils; induction machine; maximum efficiency operation; maximum torque per ampere operation; phase-changing; pole-changing

Citation: Bitsi, K.; Bosga, S.G.; Wallmark, O. Design Aspects and Performance Evaluation of Pole-Phase Changing Induction Machines. *Energies* **2022**, *15*, 7012. https://doi.org/10.3390/en15197012

Academic Editor: Frede Blaabjerg

Received: 24 August 2022
Accepted: 19 September 2022
Published: 24 September 2022

1. Introduction

The expanding electric vehicle market facilitates the technological transition towards more energy sustainable means of transportation. In the framework of this transition, the impact of the electric motor and drivetrain design becomes of paramount importance [1,2]. Such a process involves highly coupled and conflicting criteria regarding cost, torque and power density, efficiency and range, as well as strict spatial and operational constraints, such as mass and footprint [3–5].

Permanent magnet synchronous motors, and especially the interior permanent magnet topology, are extensively selected for automotive applications as they offer high torque density and efficiency and a wide-flux weakening range [6–8]. Induction machines (IMs) constitute a viable choice due to their lower cost, robustness, high overload capability and lack of rare-earth materials [9–11]. However, they inherently exhibit poorer flux weakening behavior in terms of reduced high-speed torque and power, linked to high values of leakage inductance. Several approaches have been proposed to tackle this issue, based either on leakage-minimization oriented design procedures [12,13] or torque-speed envelope manipulation methods, based on dynamic excitation schemes. The latter can range from a star-delta pole-changing Dahlander circuit [14] to electronic pole-changing. Electronic pole-changing refers to the technique of utilizing the converter in order to change

the pole number of the machine dynamically. In [15–18], the distributed windings of 3- and 6-phase IMs, respectively, are reconfigured in appropriate phase belts, rendering the change of the number of poles from four to two feasible, and the achievement of an extended flux-weakening region. The drawbacks of such winding operations are the lower fundamental winding factor and consequently lower resulting torque capability. The concept of an IM with a stator cage winding, composed of solid aluminum bars in every stator slot, short-circuited at one axial end is discussed in [19]. The use of solid stator-cage conductors naturally results in a higher fill factor; however, this topology is based on a low voltage level of 48 V, that unavoidably incurs very high current levels in the DC supply [20]. Such a concept requires that both the converter and battery systems need to be redesigned to voltage levels much lower than the standard ones used in the electric vehicle market today [21], while the effect of so high current levels in the overall drive system needs careful investigation.

The wound independently-controlled stator coils (WICSC) machine is presented in [22]. Its geometry is shown in Figure 1a. The configuration of the stator-winding in this topology enables the individual energization and control of the coils in each stator slot, facilitating the real-time change of both phase and pole number during operation. As a result, the WICSC machine is compatible with the current high-voltage battery systems and semiconductors, while the presence of individually excited coils in each slot offers high degree of freedom in the applied excitation scheme, with the capability of maximizing the fundamental winding factor, when the number of stator slots per pole per phase is set to unity. Similar concepts are preliminary explored in [23,24]. Initial attempts of electronic pole-changing are explored also in [25], where an IM with wound toroidal coils is combined with a 9-phase inverter in an integrated starter generator application. In [26,27], generalized dynamic and steady-state models of pole-changing IMs are proposed. In [28], different pole-selection strategies for the operation of a variable-pole toroidally-wound IM are investigated. However, the authors impose a 'flux-linkage limit' in the analysis of the different pole-phase modes, presenting therefore a comparison based on a lower saturation basis. This approach could incur an artificially induced early saturation of the magnetizing current for the low-pole operations, that may result in unfair favoring of the high-pole count operations, especially in the original 2-pole prototype measured in [28].

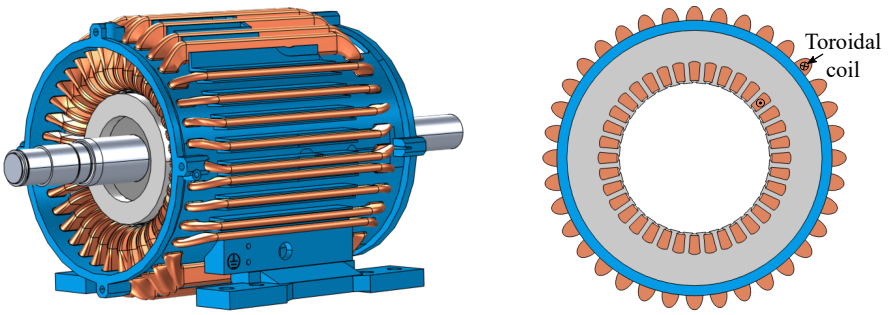

(**a**) (**b**)

Figure 1. (**a**) 3D model of the WICSC machine and (**b**) 2D schematic of the stator yoke, the housing and the independent coils.

The design of pole-phase changing IMs constitutes a complicated problem, as it inherently couples electromagnetic design and control variables. The limited literature on the subject does not include any complete and generic design procedure, or any sensitivity analysis to quantify the effect of design variables on the full utilization of the pole-phase changing capability and the optimal split of the operating range into different pole-phase modes. The aim of this paper is to provide useful insight in the benefits and design limitations of different pole-phase changing IM operations. For this purpose, two WICSC machine geometries are analyzed based on their pole-phase changing behavior. These geometries correspond to machines that were originally designed for fixed pole-phase

operation, with two and six magnetic poles, respectively. The focus of the study is on the ability of the two designs to maximize the torque capability, efficiency and flux-weakening range compared to their fixed pole-phase counterparts. The performance of each possible pole-phase combination is estimated and thoroughly analyzed at each operating point in the entire operating region. These results are compared for both examined machine designs and the optimal operations are determined. This detailed analysis showcases how the utilization of higher pole-operations can result in notably higher maximum torque capability and efficiency at lower speeds, while lower pole operations offer a significant extension of the field weakening range and the available peak power at the maximum speed. This work validates the importance of pole-phase changing IMs and serves as a guideline towards the standardization of the pole-phase changing IM design process.

The outline of this paper is as follows. In Section 2, the principles of pole-phase changing IMs are discussed and the key role that saturation plays in these IMs is thoroughly explained. Section 3 analyzes the optimal pole-phase selection processes that should be followed for different operating strategies, i.e., maximum torque per ampere and maximum efficiency operation. In Section 4, the design considerations of pole-phase changing IMs are discussed based on the pole-phase changing performance of the original 2-pole and original 6-pole machines. Conclusions are drawn in the last section.

2. Working Principles of Pole-Phase Changing Induction Machines

The stator yoke of the WICSC machine is shown in Figure 1b. In each slot, a toroidal coil is wound axially around the stator yoke. Each stator-slot coil is connected to a separate converter leg, thus can be independently supplied and controlled. The advantage of the individually-excited coils is the inherent ability to change arbitrarily the stator-current excitation scheme on demand. This facilitates the real-time change of the number of active phases and poles during operation.

2.1. Multiphase Stator Winding Excitation

In this analysis, a balanced, sinusoidal m-phase current excitation is considered in the stator winding. Thus, the current in each phase n, $i_{s,n}$ can be expressed as [22]

$$i_{s,n} = \hat{\imath}_s \cos\left(\frac{p}{2}\omega_s t - (n-1)\frac{\pi}{m}\right) \tag{1}$$

where $\hat{\imath}_s$ is the stator current amplitude, ω_s is the angular electrical frequency, t is the time, m is the number of phases and p is the number of poles. The number of stator slots per pole per phase q_s is by definition

$$q_s = \frac{Q_s}{mp} \tag{2}$$

where Q_s is the number of stator slots. In order to maximize the winding factor and by extension to minimize the harmonic content, q_s is selected equal to 1 in this study. Therefore, for a given pole number, the highest possible phase number will be chosen for the supplied current excitation according to (2), as these are the configurations of interest for phase-pole modulation.

2.2. Torque Capability in Linear and Saturation Region

The steady-state electromagnetic torque T_e of the WICSC machine, as a contribution of the fundamental space harmonic, can be expressed in the linear region as

$$T_e = \frac{mp}{2}\lambda_{sd} i_{sq} = \frac{mp}{2} L_m i_{sd} i_{sq} \tag{3}$$

where λ_{sd} is the d-axis stator flux linkage and i_{sd} and i_{sq} are the d- and q-axis stator currents, respectively, in the rotor-flux reference frame. Moreover, L_m is the magnetizing inductance, approximated by

$$L_m = \frac{2\mu_0 {n_s}^2 {Q_s}^2 L_a r_r k_1}{\pi \delta p^2 m} \tag{4}$$

where μ_0 is the vacuum permeability, n_s is the number of turns per stator slot, L_a is the active axial length, r_r is the rotor radius, k_1 is the fundamental winding factor and δ is the air-gap length [22].

According to (3) and (4), the maximum torque per ampere (MTPA) capability is inversely proportional to the number of poles. Thus, the higher the number of selected poles, the higher the required current to attain the same torque capability. This linear behavior between torque and number of poles can be observed in Figure 2a in a 2-pole general purpose IM. The motor is operated at constant mechanical speed $n = 500$ rpm and stator current $\hat{\imath}_s = 2$ A in all pole-phase operations. As expected, since saturation and skin effect are almost negligible at this operating point, the maximum torque occurs at MTPA current angles close to 45° [29]. In addition, an inversely proportional relationship between the magnetic flux density in the air-gap B_δ and the number of poles is evident. This relation can be formulated as follows [30]

$$B_\delta = \frac{\mu_0 Q_s k_1 n_s i_m}{\pi p \delta} \tag{5}$$

where i_m is the magnetizing current, which is equal to i_{sd}. However, the above observation no longer holds once magnetic saturation becomes apparent in the ferromagnetic parts of the WICSC machine. This is exemplified in Figure 2b. The motor now is operated at constant mechanical speed $n = 500$ rpm and stator current $\hat{\imath}_s = 5$ A. Since an increase in i_m no longer results in an equally large increase in T_e as it would in the linear region, an increase in torque is now more beneficially obtained by increasing i_{sq}. As it can be observed, the output torque capability, T_e, is no longer proportional to the supplied current and the inverse of the number of poles, as in the linear region.

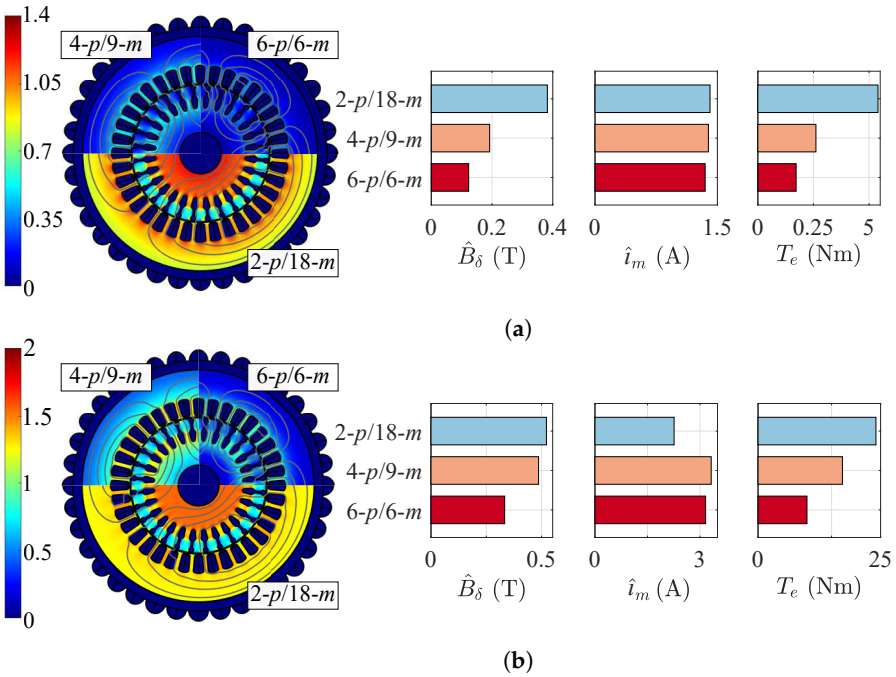

Figure 2. Comparison of the magnetic flux distribution, the air-gap magnetic induction amplitude $\hat{B}_\delta$, the magnetizing current amplitude $\hat{\imath}_m$ and the maximum torque capability T_e for different pole-phase operations in (**a**) the linear region ($\hat{\imath}_s = 2$ A) and (**b**) the saturation region ($\hat{\imath}_s = 5$ A).

In conclusion, saturation plays a vital role in the performance of a pole-phase changing IM. Therefore, in order to accurately predict the overall capabilities of the different pole-phase operations, the local saturation that takes place in the different parts of the machine has to be thoroughly characterized. Only then can a pole-phase changing IM be effectively designed and sensibly utilized in the entire operating region.

3. Optimal Pole-Phase Selection Process

To optimally operate the WICSC machine, the appropriate selection process among all the possible pole-phase combinations should be determined. As it was shown in Section 2, the performance of each pole-phase mode is constrained by various limiting factors, rendering no specific mode superior unequivocally in the entire operating region. The key in this process is the identification of the suitable operation at all necessary operating points based on the imposed requirements. These requirements can be aiming at various targets, such as the maximization of the torque capability, the minimization of the power losses, the optimal post-fault operation or the overall performance enhancement by utilizing harmonic injection. This paper will focus on two different operating strategies: (a) maximization of the torque per ampere capability, and (b) maximization of the machine efficiency.

3.1. Maximum Torque Per Ampere Operation

The goal of this strategy is to maximize the operational torque-speed envelope of the machine. In order to determine at each specific operating point the pole-phase operation that results in the highest torque per ampere output, first, the maximum torque capabilities of all operations need to be specified. This can be achieved by adopting the following current-control schemes: MTPA control, flux weakening (FW) control and maximum torque per volt (MTPV) control.

3.1.1. Maximum Torque Per Ampere (MTPA) Control

At low speeds, where the WICSC machine operates at voltages lower than the maximum permissible value $V_{\max}$ imposed by the DC bus voltage limit, i_s is the only factor limiting the produced torque output. Thus, the MTPA control is used. When i_s is low and the machine operates in the linear region, the angular slip frequency ω_{slip} can be calculated in the rotor-flux reference frame as

$$\omega_{\text{slip}} = s\omega_s = \frac{R'_r}{L_m}\frac{i_{sq}}{i_{sd}} \tag{6}$$

where s is the slip and R'_r is the rotor resistance referred to the stator side in the steady-state equivalent circuit of the IM model [31]. (6) can be utilized to determine the optimal slip of the machine under MTPA control. The developed algorithm for maximum torque per ampere operation uses as a starting point this analytical slip estimation. Then, it performs a number of FEM simulations with small variations of the slip, in order to determine numerically the optimal slip that results in the maximum torque output. As it was demonstrated in Section 2, at higher i_s levels, where saturation becomes more prominent, the MTPA current angle gradually increases to values higher than 45°. In addition, the iron behaves non-linearly and the parameters are no longer constant, with a gradual decrease in the inductance values [29]. As a result, an increase in i_s causes an increase in the MTPA slip frequency. A maximum current constraint is defined by the converter current rating.

3.1.2. Flux Weakening (FW) Control

The FW control is adopted once the DC bus voltage limit is reached. In order to operate at higher speeds, while maintaining the voltage constant and equal to $V_{\max}$, the produced stator flux λ_{sd} needs to be reduced. Therefore, the current angle should be increased. Using this method, the WICSC machine can reach the required speeds at the expense of a lower maximum torque capability.

3.1.3. Maximum Torque Per Volt (MTPV) Control

If it is unfeasible to respect both the current and voltage limits above a certain speed in the high-speed region, the MTPV control should be used. The machine must be operated at lower current levels in order to further decrease the stator flux λ_{sd}. Thus, the slip frequency should be reduced in similar fashion in order to output the maximum torque while still being restricted by the voltage limit.

Using the above current-control schemes, for each pole-phase operation a torque-speed envelope is obtained as a function of the available i_s. By combining the results from the different operations, the envelope for the WICSC machine is found.

3.2. Maximum Efficiency Operation

The optimal efficiency of the WICSC machine can be evaluated by considering and numerically computing the major loss components. These include:

3.2.1. Resistive Losses

The stator copper losses $P_{\mathrm{Cu},s}$ can be estimated as follows

$$P_{\mathrm{Cu},s} = \frac{Q_s}{2} \hat{i}_s^2 R_{s,\mathrm{coil}} \tag{7}$$

where $R_{s,\mathrm{coil}}$ is the resistance of each stator-slot coil, which is computed assuming that the stator-slot coil has a constant temperature of 80 °C, while excluding skin and proximity effects. It should be noted that the stator-coil end-winding resistance and inductance are included in the numerical analysis, by properly assigning an external electric circuit to each individual coil in the 2D finite-element-method (FEM) model. The end-winding inductances are estimated by manipulating the expression for an air-cored solenoid inductance to take into account the presence of iron parts in the vicinity [32].

The losses dissipated in the aluminum squirrel-cage rotor $P_{\mathrm{Al},r}$ are calculated using the following expression

$$P_{\mathrm{Al},r} = \frac{Q_r}{2} \hat{i}_r^2 R_r \tag{8}$$

where $\hat{i}_r$ is the rotor-bar current amplitude, Q_r is the number of rotor bars and R_r is the equivalent rotor-bar resistance, corresponding to the resistance of one bar and two short-circuit ring elements

$$R_r = R_b + \frac{2R_{\mathrm{scr}}}{\sin^2\left(\frac{\pi p}{Q_r}\right)} \tag{9}$$

where R_b is the rotor-bar resistance and R_{scr} is the resistance of one short-circuit ring element [33]. The aluminum resistivity is calculated assuming that the rotor bars and short-circuit ring operate at a constant temperature of 100 °C. In a similar fashion as in the stator, the resistances and the inductances of the short-circuit ring elements are added in the FEM model using an external electric circuit to properly short circuit the rotor bars. The end-winding squirrel-cage inductance is approximated using analytical formulas to calculate the self-inductance of an identical circular ring, as described in [34].

3.2.2. Iron Losses

For the estimation of the iron losses of the WICSC machine, the magnetic flux density is numerically computed in each mesh element κ in the stator and rotor core, and expressed as a Fourier series expansion in a spectrum of frequencies as

$$B_\kappa(t) = \sum_{\nu=1}^{\infty} |B_{\kappa,\nu}| \cos[\omega_\nu t + \arg(B_{\kappa,\nu})] \tag{10}$$

where $B_{\kappa,\nu}$ is the complex Fourier coefficient of the magnetic flux density in the mesh element κ and ω_ν is the angular electrical frequency, both at frequency f_ν [35]. The total iron losses P_{Fe} in the ferromagnetic parts of the machine can be calculated as

$$P_{\mathrm{Fe}} = L_a \sum_{\kappa=1}^{\kappa_{\max}} \sum_{\nu=1}^{\nu_{\max}} \Big\{ k_{\mathrm{e}}(|B_{\kappa,\nu}|) f_\nu^2 |B_{\kappa,\nu}|^2 + k_{\mathrm{h}}(|B_{\kappa,\nu}|) f_\nu |B_{\kappa,\nu}|^2 \Big\} \Delta_\kappa \tag{11}$$

where k_{e} and k_{h} are the eddy-current and hysteresis loss coefficients, respectively, and Δ_κ is the area of the mesh element κ. The loss coefficients are considered to be a function of the magnetic flux density and are approximated as third-order polynomials [36].

3.2.3. Windage Losses

To approximate the windage losses P_w, the following empirical formula is used

$$P_w = C_D \pi \rho r_r L_\alpha {\nu_r}^3 \tag{12}$$

subject to

$$\sqrt{C_D} = 2.04 + 1.768 \ln\left(\mathrm{Re}\sqrt{C_D}\right)$$
$$\mathrm{Re} = \frac{\rho}{\mu} \omega_m r_r \delta \tag{13}$$

where C_D is the skin friction coefficient, ρ is the air density, ν_r is the rotor surface speed, μ is the kinematic viscosity of air, Re is the Reynolds number and ω_m is the angular mechanical frequency [37].

Based on (7)–(13), the efficiency η of the examined pole-phase operations can be determined numerically at each operating point using the following expression:

$$\eta = \frac{P_m}{P_m + P_{\mathrm{Cu},s} + P_{\mathrm{Al},r} + P_{\mathrm{Fe},s} + P_{\mathrm{Fe},r} + P_w}. \tag{14}$$

where P_m is the mechanical power and $P_{\mathrm{Fe},s}$ and $P_{\mathrm{Fe},r}$ is the stator and rotor iron losses, respectively. Within the torque-speed envelope for the maximum current i_s, as obtained according to the previous section, at each point for each possible operation the efficiency has thus been calculated. The operation with best efficiency is then chosen and recorded in the optimal efficiency map of the machine.

4. Design Considerations

The design of a pole-phase changing IM is a rather challenging task. There are many factors to be taken into consideration to maximize the potential benefits compared to a fixed pole-phase topology. In order to highlight the importance of this process, two machine topologies are presented and compared based on their pole-phase changing behavior. These topologies are shown in Figure 3 and correspond to machines that were originally designed for fixed pole-phase operation, with two and six magnetic poles, respectively. The 2-pole design is an off-the-shelf machine, while the 6-pole geometry was designed in the scope of this analysis in order to have as fixed pole-phase machine the same original nominal operating point, rotor-bar current densities as well as outer dimensions (i.e., active length L_α and stator outer diameter D_o) with the 2-pole design. The rotor short-circuit ring dimensions were selected in this geometry by assuming equal current density in the ring as in the rotor bars when operated according to the design pole operation. The analysis has been carried out numerically using 2D FEM models, supplied with sinusoidal stator current excitation.

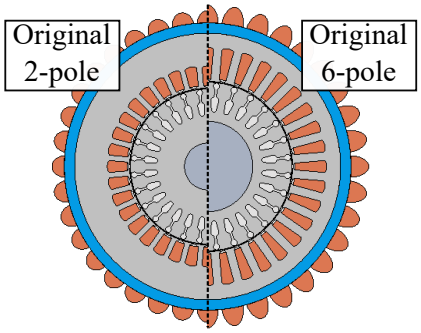

Figure 3. Investigated WICSC IMs, originally designed for 2-pole and 6-pole fixed pole-phase operation.

4.1. WICSC Machine Designed for 2-Pole Nominal Operation

The pole-phase changing behavior of an off-the-shelf 20 kW, 64 Nm, 3000 rpm, original 2-pole IM is examined. In order to observe the overloadability and the impact of pole-phase changing at high-load operation, the current limit is set to $\hat{\imath}_{s,\max} = 22$ A. This limit translates to maximum 2.5 times the original rated torque, a level that can be reached for short-time operation, since the machine is still not heavily saturated. Furthermore, the DC bus voltage limit is 300 V, which corresponds to a machine voltage limit of $V_{\max} = 150$ V by using the m-phase bridge-type voltage-source converter topology considered in [22].

4.1.1. Maximum Torque Per Ampere Operation

Using maximum torque per ampere strategy, the performance of the different pole-phase operations at $n = 500$ rpm is shown in Figure 4. It should be noted that, in contrast to the typical control method of an IM, after reaching the original nominal operating point, $\hat{\imath}_m$ is not kept constant. The sole aim of this strategy is to maximize the torque per ampere output and, therefore, no flux-linkage constraints are imposed (below the $V_{\max}$ limit).

As the excitation levels are increasing, the 2-pole operation requires the lowest $\hat{\imath}_m$ to give rise to a comparatively high $\hat{B}_\delta$, thus allowing for higher torque production. In the 4-pole operation, the local saturation in the stator and rotor teeth plays a hindering role in the growth of $\hat{B}_\delta$, and in combination with the requirement of an increased $\hat{\imath}_m$, it is only at the highest excitation levels that the 4-pole succeeds in having a better torque capability than the 2-pole operation, as depicted in Figure 4g.

The resulting optimal torque-speed map for maximum torque per ampere operation is shown in Figure 5. The favorable pole number changes from 2 to 4 at approximately 2 times the original nominal torque of the topology. At around 2400 rpm for the 4-pole operation, the $V_{\max}$ limit is reached, which leads to a gradual decrease of the maximum torque output and the resulting superiority of the 2-pole at $n = 2645$ rpm. The rest of the higher pole operations do not manage to reach higher torque per ampere levels (see Figure 4h) and, therefore, are excluded from the optimal torque per ampere operation of this geometry. From Figure 5, it becomes clear that if the examined machine is operated with a current limit of 18 A or lower, there is not a single operating point where pole-phase changing extends the torque-speed envelope of the machine.

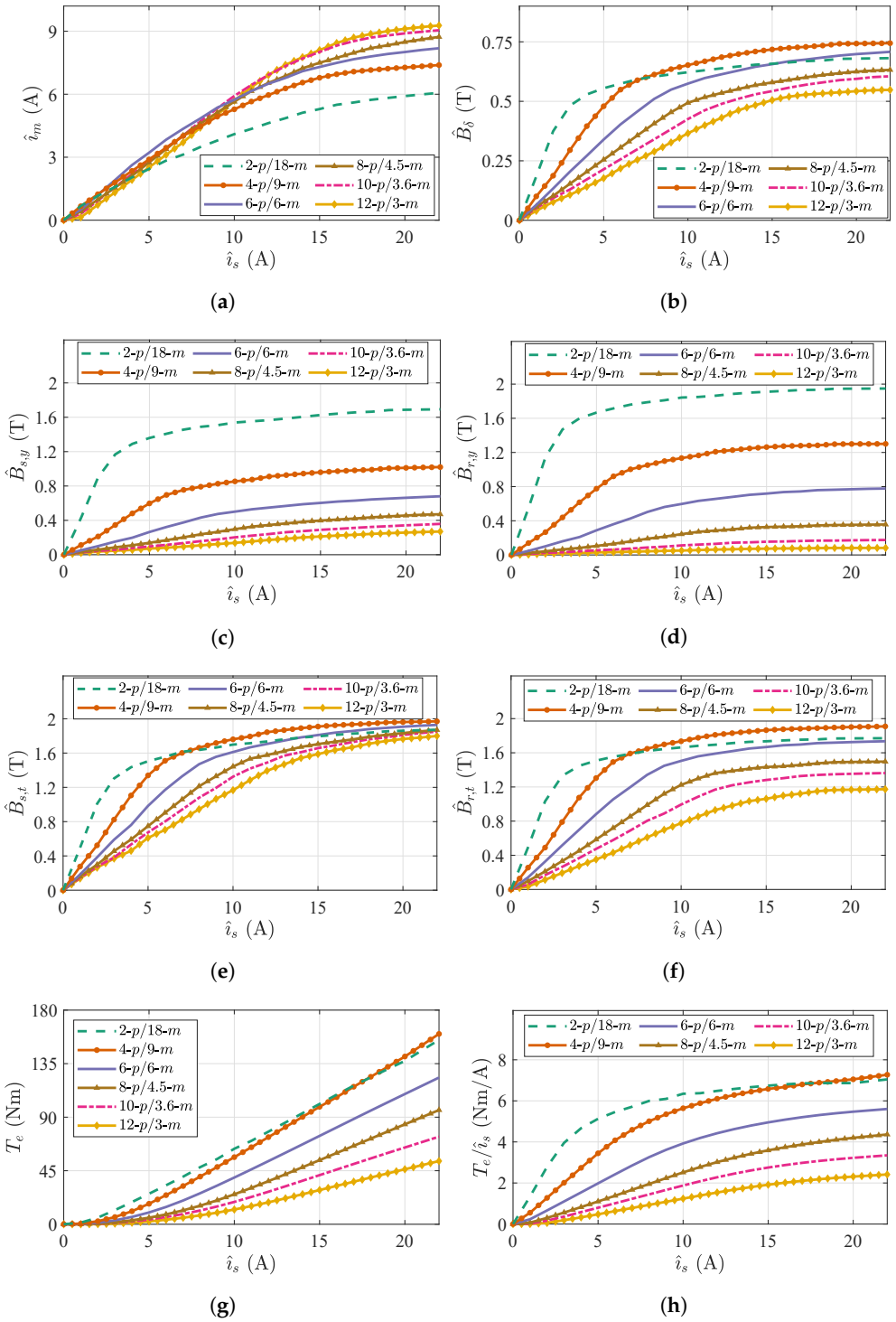

Figure 4. Plots of $\hat{i}_s$ vs. (**a**) $\hat{i}_m$, (**b**) $\hat{B}_\delta$, (**c**) stator-yoke magnetic flux density amplitude $\hat{B}_{s,y}$, (**d**) rotor-yoke magnetic flux density amplitude $\hat{B}_{r,y}$, (**e**) stator-tooth magnetic flux density amplitude $\hat{B}_{s,t}$, (**f**) rotor-tooth magnetic flux density amplitude $\hat{B}_{r,t}$, (**g**) T_e and (**h**) $T_e/\hat{i}_s$ at $n = 500$ rpm for different pole-phase operations of an original 2-pole machine at maximum torque per ampere operation.

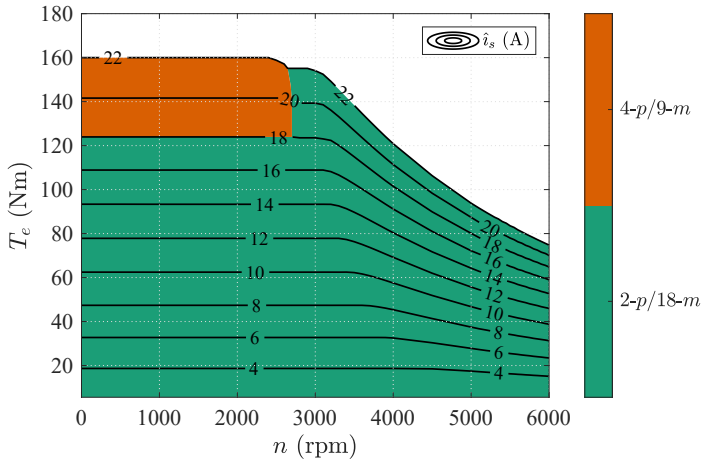

Figure 5. Optimal torque-speed map of an original 2-pole machine operated as pole-phase changing machine with maximum torque per ampere strategy.

4.1.2. Maximum Efficiency Operation

As a next step, the maximum efficiency strategy is adopted and the benefits of pole-phase changing in terms of maximizing the efficiency over the entire torque-speed range are observed. The various loss components of the different pole-phase operations at $n = 1500$ rpm are demonstrated in Figure 6. It can be seen that, at this speed, the 4-pole operation produces the lowest total losses P_l above $T_e = 73$ Nm, while adhering to maximum efficiency control, rendering this operation superior at the highest current excitations. Comparing 2- and 4-pole operation in Figure 6g,h, it can be seen that changing from 2- to 4-pole operation shifts a portion of the total losses from the rotor to the stator. As stator cooling is typically easier than rotor cooling [38], it can be understood that 4-pole operation can enhance the torque capability of the machine.

In Figure 7, the optimal efficiency map is depicted. Whereas changing to a higher pole number only slightly extends the torque-speed envelope of the machine (at low speed, and only at a current limit higher than 18 A), changing to 4-pole operation is interesting from an efficiency point of view in a significant part of the operating range of the machine. The explanation for this is found in the rotor copper losses that are significantly lower in the 4-pole operation, whereas only at higher speeds the higher (stator) iron losses compensate for this difference.

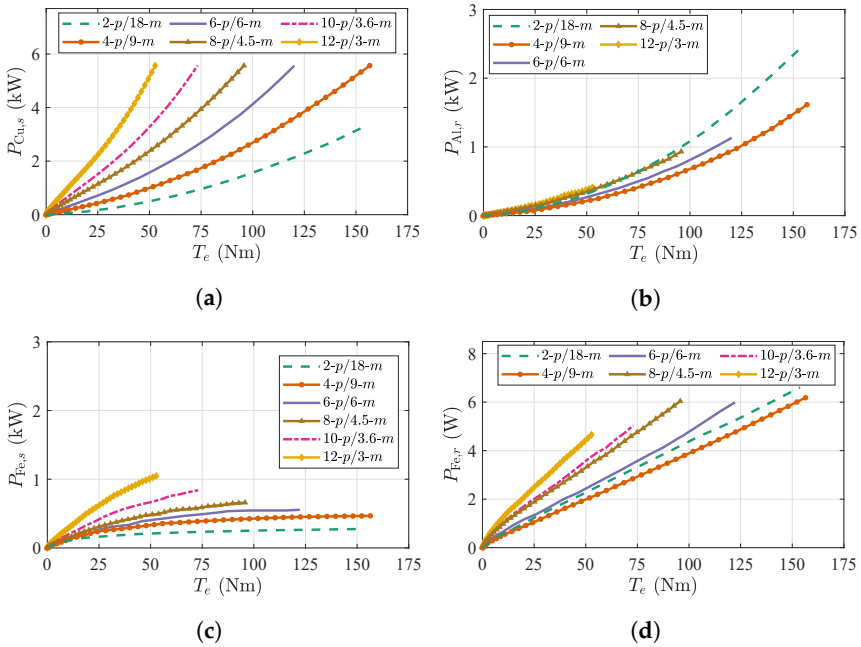

Figure 6. *Cont.*

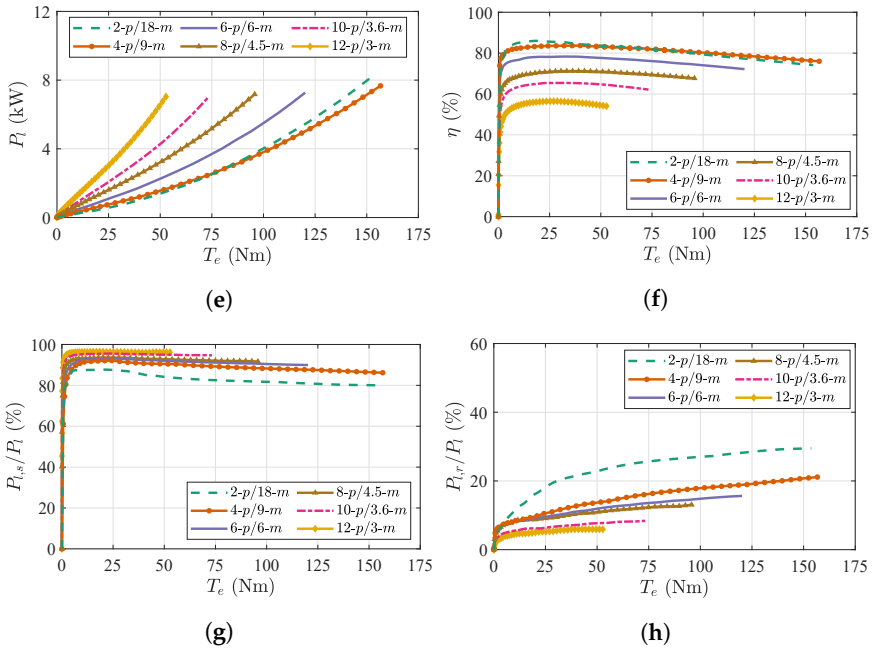

Figure 6. Plots of T_e vs. (**a**) $P_{\mathrm{Cu},s}$, (**b**) $P_{\mathrm{Al},r}$, (**c**) $P_{\mathrm{Fe},s}$, (**d**) $P_{\mathrm{Fe},r}$, (**e**) total losses P_l, (**f**) η, (**g**) percentage of total stator losses over total losses $P_{l,s}/P_l$ and, (**h**) percentage of total rotor losses over total losses $P_{l,r}/P_l$ at $n = 1500$ rpm for different pole-phase operations of an original 2-pole machine at maximum efficiency operation.

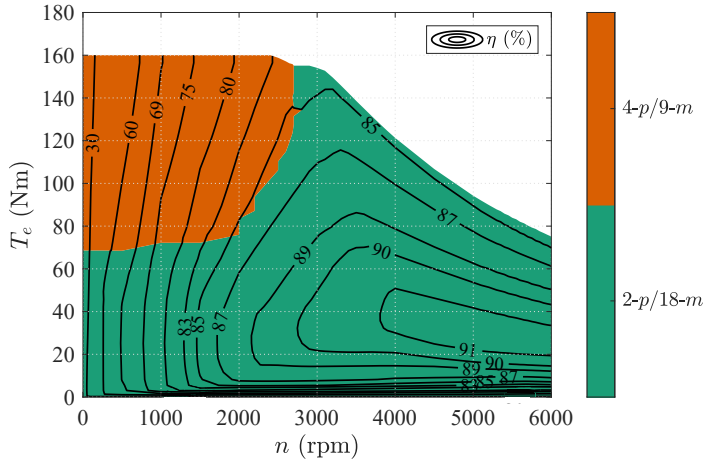

Figure 7. Optimal efficiency map of an original 2-pole machine operated as pole-phase changing machine with maximum efficiency strategy.

4.2. WICSC Machine Designed for 6-Pole Nominal Operation

The next investigated geometry is an original 20 kW, 64 Nm, 3000 rpm, 6-pole IM. Along with the same original nominal operating point, the goal during the design phase of this machine was to keep the same outer dimensions and rotor-bar current density as in the 2-pole design analyzed in the previous section. In addition, the number of turns of this design was selected with the target of achieving equivalent torque per ampere capability with the original 2-pole IM at the nominal excitation, and thus comparable torque-speed envelopes.

4.2.1. Maximum Torque Per Ampere Operation

The resulting performance of the different pole-phase operations with maximum torque per ampere strategy at $n = 500$ rpm is shown in Figure 8. In this topology, a beneficial shift can be observed from the lowest pole number (i.e., 2) at low stator currents,

to gradually higher pole numbers as the excitation is increased. Although the 2-pole and 4-pole operations impose the lowest demands of $\hat{\imath}_m$, at the same time, the produced $\hat{B}_\delta$ and by extension the torque per ampere output, remain relatively low, greatly affected by local saturations present in the stator and rotor yoke. On the contrary, saturation seems to impact the torque per ampere levels of the 6-pole only at the highest excitations of the examined range, where the 8-pole topology yields the best torque output.

The optimal torque-speed map for maximum torque per ampere operation is depicted in Figure 9. In this case, the extension of the torque-speed envelope by utilizing pole-phase changing is more profound. On the one hand, with a current limit of 20 A or higher, the 8-pole operation produces an up to 12% higher torque capability than the 6-pole at speeds below 1680 rpm. On the other hand, the lower pole-number operations (i.e., 2-pole and 4-pole) significantly widen the flux weakening range compared to a fixed 6-pole operation. An interesting phenomenon is noted in particular in the speed range from 3880 to 6000 rpm, where the optimal pole number first changes from 2 to 4, as the 4-pole operation has the better torque-per-ampere capability, and then back to 2 pole, as the voltage limit restrains the torque in 4 pole operation.

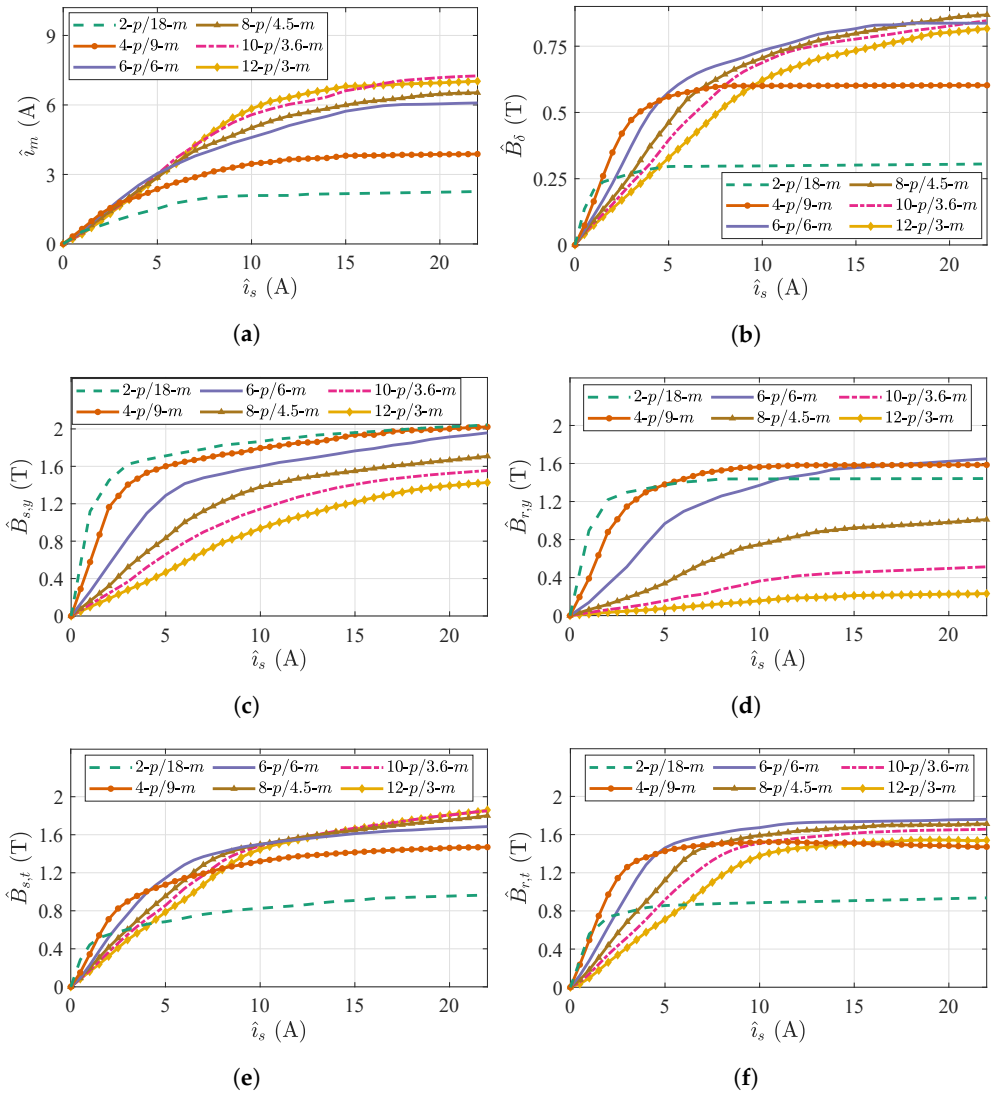

Figure 8. *Cont.*

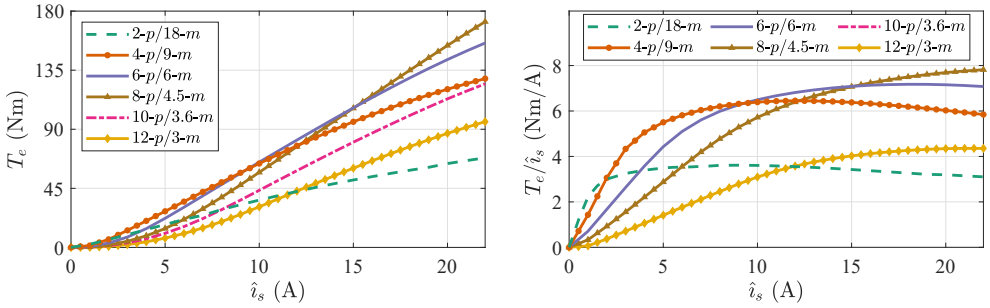

(**g**) (**h**)

Figure 8. Plots of $\hat{\imath}_s$ vs. (**a**) $\hat{\imath}_m$, (**b**) $\hat{B}_\delta$, (**c**) $\hat{B}_{s,y}$, (**d**) $\hat{B}_{r,y}$, (**e**) $\hat{B}_{s,t}$, (**f**) $\hat{B}_{r,t}$, (**g**) T_e and (**h**) $T_e/\hat{\imath}_s$ at $n = 500$ rpm for different pole-phase modes of an original 6-pole machine at maximum torque per ampere operation.

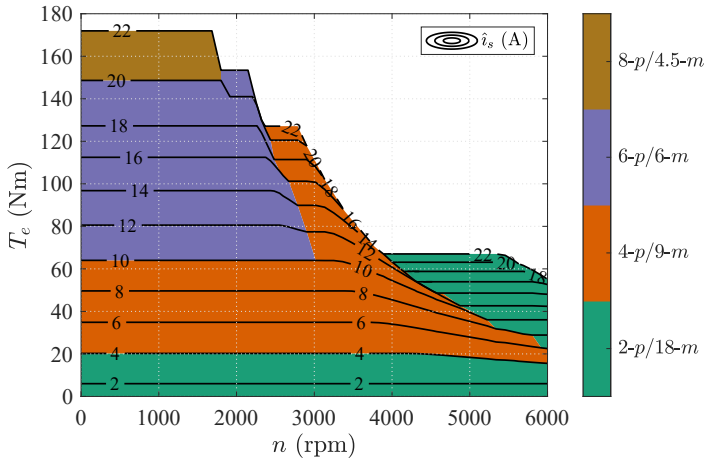

Figure 9. Optimal torque-speed map of an original 6-pole machine operated as pole-phase changing machine with maximum torque per ampere strategy.

4.2.2. Maximum Efficiency Operation

Employing maximum efficiency strategy, the estimated loss components of the different pole-phase operations at $n = 1500$ rpm are shown in Figure 10. With increasing current excitation, the optimal pole selection changes from 2 to 4, 6 and finally 8 at the torque levels of 9.5 Nm, 73 Nm and 105 Nm, respectively.

Taking into consideration the entire speed range, the optimal torque-speed map for maximum efficiency operation is shown in Figure 11. As it can be observed, the low pole-number operations manage to both extend the flux-weakening range considerably and also to improve the efficiency of the machine. In addition, here, we note a speed range where 2-pole operation is beneficial at both low torque levels (improved efficiency) and high torque levels (extended torque range) with 4-pole operation in-between.

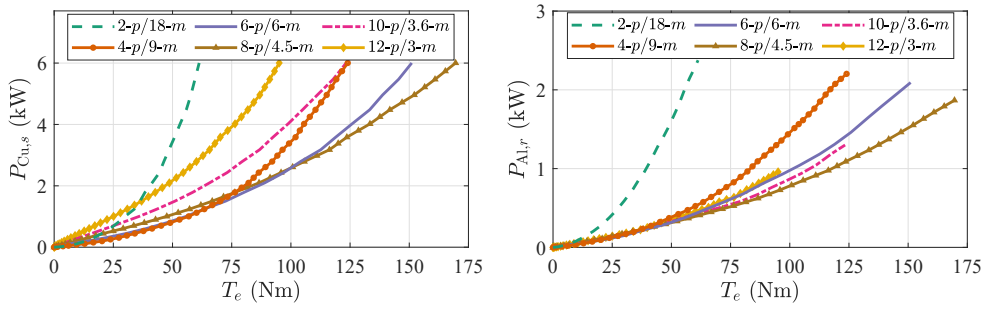

(**a**) (**b**)

Figure 10. *Cont.*

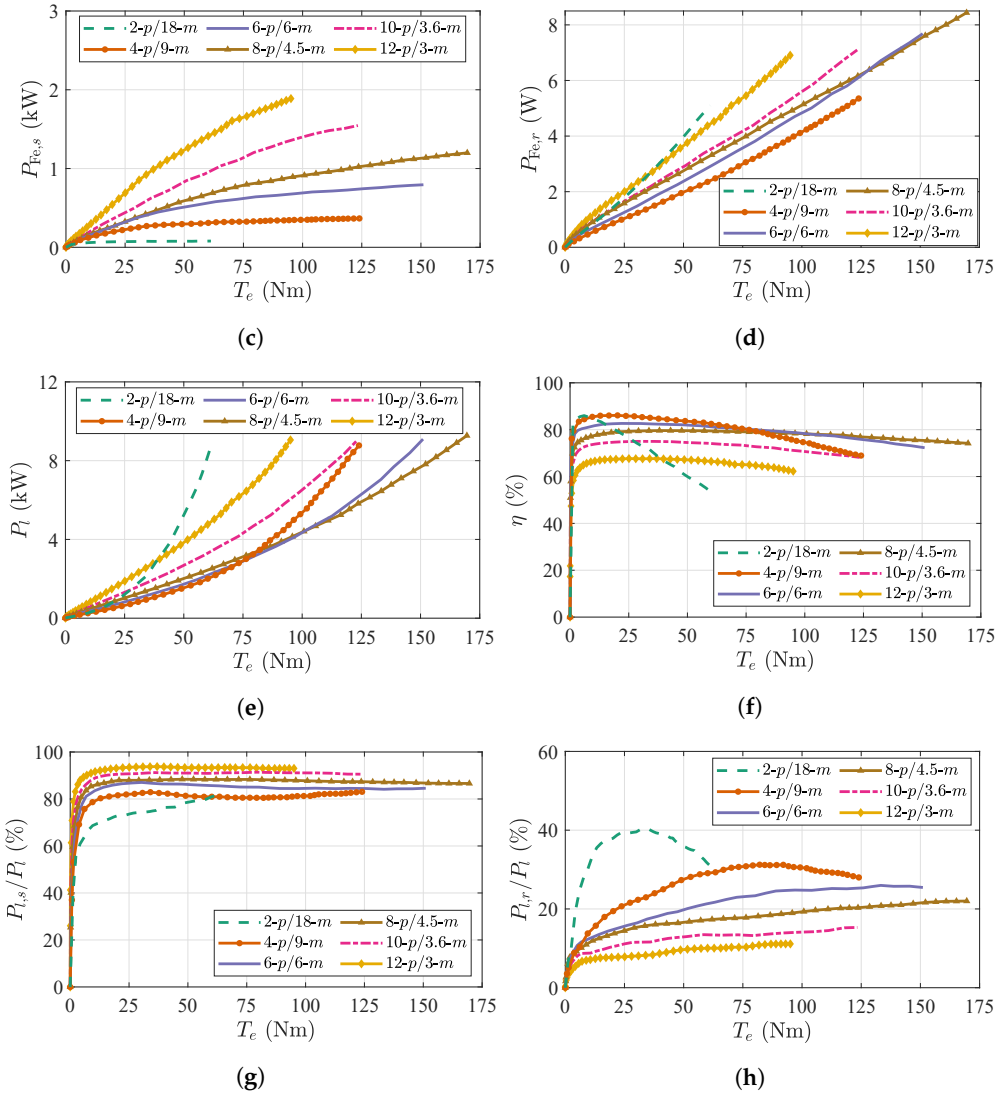

Figure 10. Plots of T_e vs. (**a**) $P_{\mathrm{Cu},s}$, (**b**) $P_{\mathrm{Al},r}$, (**c**) $P_{\mathrm{Fe},s}$, (**d**) $P_{\mathrm{Fe},r}$, (**e**) P_l, (**f**) η, (**g**) $P_{l,s}/P_l$, and (**h**) $P_{l,r}/P_l$ at $n = 1500$ rpm for different pole-phase modes of an original 6-pole machine at maximum efficiency operation.

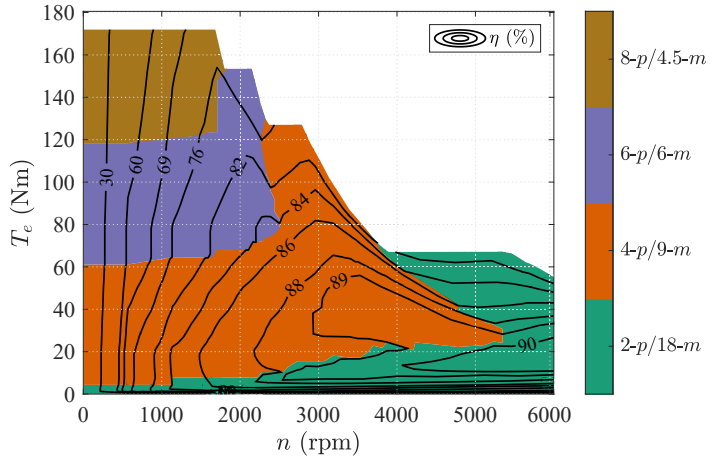

Figure 11. Optimal efficiency map of an original 6-pole machine operated as pole-phase changing machine with maximum efficiency strategy.

5. Discussion

As it is shown in Section 4, pole-phase changing can offer significant advantages depending on the design of the machine. The presented findings of this study can be recapitulated as follows. For the original 2-pole IM, it is found that the 4-pole operation under maximum torque per ampere strategy extends to a small degree the available torque only in a range below base speed and at relatively high current levels. However, when the maximum efficiency strategy is followed, there is a significant part of the torque-speed range where 4-pole operation improves the machine efficiency as compared to 2-pole operation. Furthermore, 4-pole operation is noted to affect significantly the distribution of total losses between the rotor and the stator. Even at operating points where the 2-pole operation demonstrates superior efficiency, switching to 4-pole operation may still be beneficial in cases where the rotor cooling is a limiting factor. Finally, it is found that operation of the original 2-pole machine with pole numbers higher than 4 does not provide any benefit at all at the studied power range.

For the IM designed originally as a 6-pole, the operation with different pole numbers offers significantly more benefits. Whereas there is a small extension in peak torque below base speed with 8-pole operation under maximum torque per ampere strategy, gradually switching to lower pole numbers results in a significant extension of torque at high speed. Moreover, switching to lower pole numbers allows operation with lower stator current for a given torque in the entire speed range in partial load conditions. When the maximum efficiency strategy is applied, it is noted that in the largest part of the torque-speed map 4-pole operation results in the best efficiency. At low load levels as well as at high speed, 2-pole operation exhibits the highest efficiency. In addition, for this machine design, 6- and 8-pole operations are the best in terms of efficiency in the low-speed/high-torque region. Furthermore, a notable percentage of total losses is shifted from the stator to the rotor with operations with higher pole number than 2, thus improving the dynamic overloadability of the machine. Finally, there are no advantages in using pole numbers higher than 8 at the studied power range.

6. Conclusions

The goal of this paper is to evaluate the effect of pole-phase changing on the performance of two IM designs with different original design pole numbers. Two main aspects are considered: the maximization of the efficiency and the maximization of the torque capability in the entire operating range. Comparing the cases of the original 2- and 6-pole IMs, it can be concluded that there are significant differences in the degree as to which pole-phase changing improves the performance of the machine. For the original 6-pole IM, the benefits of pole-phase changing are more pronounced. The operation with reduced pole numbers significantly extends the field-weakening range of the machine and improves the efficiency at lower current levels, while the operation with 8 poles results in higher peak torque at low speeds. For the 2-pole IM, the advantages of pole-phase changing are noted in the high-torque region below base speed. Specifically, the 4-pole operation in this region results in higher efficiency and maximum torque capability, as well as a shift of a notable portion of the total losses from the rotor to the stator. It can be concluded that the design of a machine plays a crucial role to what extent pole-phase changing can ameliorate the overall efficiency, the maximum torque capability and the available field-weakening range.

Author Contributions: Conceptualization, O.W., S.G.B. and K.B.; methodology and analysis, K.B. and S.G.B.; FEM model development, K.B.; data curation and writing—original draft preparation, K.B.; writing—review and editing, S.G.B.; supervision, funding acquisition, S.G.B. and O.W. All authors have read and agreed to the published version of the manuscript.

Funding: This research project is supported in part by the Swedish Energy Agency.

Data Availability Statement: Not applicable.

Conflicts of Interest: The authors declare no conflict of interest.

Abbreviations

FEM	Finite element method
FW	Flux weakening
IM	Induction machine
MTPA	Maximum torque per ampere
MTPV	Maximum torque per volt
WICSC	Wound independently-controlled stator coils

Nomenclature

B_δ	Air-gap magnetic flux density	(T)
C_D	Skin friction coefficient	(-)
i_m	Magnetizing current	(A)
i_{sd}	*d*-axis stator current	(A)
i_{sq}	*q*-axis stator current	(A)
i_s	Stator current	(A)
$\hat{\imath}_r$	Rotor-bar current amplitude	(A)
k_1	Fundamental winding factor	(-)
k_e	Eddy-current loss coefficient	(-)
k_h	Hysteresis loss coefficient	(-)
L_a	Active axial length	(m)
L_m	Magnetizing inductance	(H)
m	Number of phases	(-)
n_s	Number of turns per stator slot	(-)
p	Number of poles	(-)
$P_{\mathrm{Al},r}$	Losses of aluminum squirrel-cage rotor	(W)
$P_{\mathrm{Cu},s}$	Stator copper losses	(W)
P_Fe	Total iron losses	(W)
$P_{\mathrm{Fe},s}$	Stator iron losses	(W)
$P_{\mathrm{Fe},r}$	Rotor iron losses	(W)
P_m	Mechanical power	(W)
P_w	Windage losses	(W)
q_s	Number of stator slots per pole per phase	(-)
Q_s	Number of stator slots	(-)
Q_r	Number of rotor bars	(-)
R_b	Rotor-bar resistance	(Ω)
Re	Reynolds number	(-)
R_scr	Resistance of one short-circuit ring element	(Ω)
$R_{s,\mathrm{coil}}$	Resistance of stator-slot coil	(Ω)
r_r	Rotor radius	(m)
R_r	Equivalent rotor-bar resistance	(Ω)
R'_r	Rotor resistance referred to the stator side	(Ω)
s	Slip	(-)
t	Time	(s)
T_e	Electromagnetic torque	(Nm)
V_max	Stator maximum voltage	(V)
δ	Air-gap length	(m)
Δ_κ	Area of the mesh element κ	(m^2)
η	Efficiency	(-)
λ_{sd}	*d*-axis stator flux linkage	(Vs)
μ	Kinematic viscosity of air	(m^2/s)
μ_0	Vacuum permeability	(H/m)
ν_r	Rotor surface speed	(m/s)
ρ	Air density	(kg/m^3)
ω_m	Angular mechanical frequency	(rad/s)
ω_s	Angular electrical frequency	(rad/s)
ω_slip	Angular slip frequency	(rad/s)

References

1. Men, X.; Guo, Y.; Wu, G.; Chen, S.; Shi, C. Implementation of an Improved Motor Control for Electric Vehicles. *Energies* **2022**, *15*, 4833. [CrossRef]
2. Verbruggen, F.J.R.; Silvas, E.; Hofman, T. Electric Powertrain Topology Analysis and Design for Heavy-Duty Trucks. *Energies* **2020**, *13*, 2434. [CrossRef]
3. Bitsi, K.; Wallmark, O.; Bosga, S. Many-objective Optimization of IPM and Induction Motors for Automotive Application. In Proceedings of the 21st European Conference on Power Electronics and Applications (EPE'19 ECCE Europe), Genova, Italy, 3–5 September 2019; pp. P.1–P.10. [CrossRef]
4. Wolff, S.; Kalt, S.; Bstieler, M.; Lienkamp, M. Influence of Powertrain Topology and Electric Machine Design on Efficiency of Battery Electric Trucks—A Simulative Case-Study. *Energies* **2021**, *14*, 328. [CrossRef]
5. Roshandel, E.; Mahmoudi, A.; Kahourzade, S.; Yazdani, A.; Shafiullah, G. Losses in Efficiency Maps of Electric Vehicles: An Overview. *Energies* **2021**, *14*, 7805. [CrossRef]
6. Wang, Y.; Bianchi, N.; Qu, R. Comparative Study of Non-Rare-Earth and Rare-Earth PM Motors for EV Applications. *Energies* **2022**, *15*, 2711. [CrossRef]
7. Kimiabeigi, M.; Widmer, J.D.; Long, R.; Gao, Y.; Goss, J.; Martin, R.; Lisle, T.; Soler Vizan, J.M.; Michaelides, A.; Mecrow, B. High-Performance Low-Cost Electric Motor for Electric Vehicles Using Ferrite Magnets. *IEEE Trans. Ind. Electron.* **2016**, *63*, 113–122. [CrossRef]
8. Gu, W.; Zhu, X.; Quan, L.; Du, Y. Design and Optimization of Permanent Magnet Brushless Machines for Electric Vehicle Applications. *Energies* **2015**, *8*, 13996–14008. [CrossRef]
9. Terzic, M.V.; Mihic, D.S.; Vukosavić, S.N. Design of High-Speed, Low-Inertia Induction Machines With Drag-Cup Rotor. *IEEE Trans. Energy Convers.* **2014**, *29*, 169–177. [CrossRef]
10. Rehman, H. Detuning Minimization of Induction Motor Drive System for Alternative Energy Vehicles. *Energies* **2015**, *8*, 9117–9136. [CrossRef]
11. Goss, J.; Popescu, M.; Staton, D. A comparison of an interior permanent magnet and copper rotor induction motor in a hybrid electric vehicle application. In Proceedings of the 2013 International Electric Machines Drives Conference, Chicago, IL, USA, 12–15 May 2013; pp. 220–225. [CrossRef]
12. Zhao, Z.; Meng, S.; Chan, C.; Lo, E. A novel induction machine design suitable for inverter-driven variable speed systems. *IEEE Trans. Energy Convers.* **2000**, *15*, 413–420. [CrossRef]
13. Oldenkamp, J.L.; Peak, S.C. Selection and Design of an Inverter-Driven Induction Motor for a Traction Drive System. *IEEE Trans. Ind. Appl.* **1985**, *IA-21*, 259–265. [CrossRef]
14. Kume, T.; Iwakane, T.; Sawa, T.; Yoshida, T.; Nagai, I. A wide constant power range vector-controlled AC motor drive using winding changeover technique. *IEEE Trans. Ind. Appl.* **1991**, *27*, 934–939. [CrossRef]
15. Osama, M.; Lipo, T. A new inverter control scheme for induction motor drives requiring wide speed range. *IEEE Trans. Ind. Appl.* **1996**, *32*, 938–944. [CrossRef]
16. Osama, M.; Lipo, T. Modeling and analysis of a wide-speed-range induction motor drive based on electronic pole changing. *IEEE Trans. Ind. Appl.* **1997**, *33*, 1177–1184. [CrossRef]
17. Mallampalli, S.; Zhu, Z.Q.; Mipo, J.C.; Personnaz, S. Six-Phase Pole-Changing Winding Induction Machines With Improved Performance. *IEEE Trans. Energy Convers.* **2021**, *36*, 534–546. [CrossRef]
18. Mizuno, T.; Suzuki, S.; Tsubboi, K.; Hirotsuka, I.; Matsuda, I. Basic principle and maximum torque characteristics of a six phase pole changing induction machine for electric vehicles. In Proceedings of the IEEE Power Convers Conference, Nagaoka, Japan, 3–6 August 1997; pp. 1–8.
19. Runde, S.; Baumgardt, A.; Moros, O.; Rubey, B.; Gerling, D. ISCAD—Design, control and car integration of a 48 volt high performance drive. *CES Trans. Electr. Mach. Syst.* **2019**, *3*, 117–123. [CrossRef]
20. Bachheibl, F.; Gerling, D. High-current, low-voltage power net. In Proceedings of the 2014 IEEE International Electric Vehicle Conference (IEVC), Florence, Italy, 17–19 December 2014; pp. 1–6. [CrossRef]
21. Baumgardt, A.; Bachheibl, F.; Patzak, A.; Gerling, D. 48V traction: Innovative drive topology and battery. In Proceedings of the 2016 IEEE International Conference on Power Electronics, Drives and Energy Systems (PEDES), Trivandrum, India, 14–17 December 2016; pp. 1–6. [CrossRef]
22. Bitsi, K.; Wallmark, O.; Bosga, S. An Induction Machine with Wound Independently-Controlled Stator Coils. In Proceedings of the 2019 22nd International Conference on Electrical Machines and Systems (ICEMS), Harbin, China, 11–14 August 2019; pp. 1–5. [CrossRef]
23. Yano, H.; Sakai, K. Integrated Motor-Controlled Independently by Multi-Inverters with Pole and Phase Changes. In Proceedings of the 21st European Conference on Power Electronics and Applications (EPE'19 ECCE Europe), Genova, Italy, 3–5 September 2019; pp. P.1–P.10. [CrossRef]
24. Zheng, Y.; Zhou, L.; Wang, J.; Ma, Y.; Zhao, J. Dynamic Startup Characteristics Analysis of Single-winding Pole Changing Line-start Canned Solid-Rotor Induction Motor with Squirrel-cage. In Proceedings of the 2019 22nd International Conference on Electrical Machines and Systems (ICEMS), Harbin, China, 11–14 August 2019; pp. 1–6. [CrossRef]

25. Miller, J.; Stefanovic, V.; Ostovic, V.; Kelly, J. Design considerations for an automotive integrated starter-generator with pole-phase modulation. In Proceedings of the Conference Record of the 2001 IEEE Industry Applications Conference, 36th IAS Annual Meeting (Cat. No.01CH37248), Chicago, IL, USA, 30 September–4 October 2001; Volume 4, pp. 2366–2373. [CrossRef]
26. Magill, M.P.; Krein, P.T.; Haran, K.S. Equivalent circuit model for pole-phase modulation induction machines. In Proceedings of the 2015 IEEE International Electric Machines & Drives Conference (IEMDC), Coeur d'Alene, ID, USA, 10–13 May 2015; pp. 293–299. [CrossRef]
27. Magill, M.P.; Krein, P.T. A dynamic pole-phase modulation induction machine model. In Proceedings of the 2015 IEEE International Electric Machines & Drives Conference (IEMDC), Coeur d'Alene, ID, USA, 10–13 May 2015; pp. 13–19. [CrossRef]
28. Libbos, E.; Ku, B.; Agrawal, S.; Tungare, S.; Banerjee, A.; Krein, P.T. Loss Minimization and Maximum Torque-Per-Ampere Operation for Variable-Pole Induction Machines. *IEEE Trans. Transp. Electrif.* **2020**, *6*, 1051–1064. [CrossRef]
29. Cai, H.; Gao, L.; Xu, L. Calculation of Maximum Torque Operating Conditions for Inverter-Fed Induction Machine Using Finite-Element Analysis. *IEEE Trans. Ind. Electron.* **2019**, *66*, 2649–2658. [CrossRef]
30. Bitsi, K.; Beniakar, M.E.; Wallmark, O.; Bosga, S.G. Preliminary Electromagnetic Sizing of Axial-Flux Induction Machines. In Proceedings of the 2020 International Conference on Electrical Machines (ICEM), Gothenburg, Sweden, 23–26 August 2020; Volume 1, pp. 284–290. [CrossRef]
31. Murata, T.; Tsuchiya, T.; Takeda, I. Vector control for induction machine on the application of optimal control theory. *IEEE Trans. Ind. Electron.* **1990**, *37*, 283–290. [CrossRef]
32. Ponomarev, P.; Alexandrova, Y.; Petrov, I.; Lindh, P.; Lomonova, E.; Pyrhönen, J. Inductance Calculation of Tooth-Coil Permanent-Magnet Synchronous Machines. *IEEE Trans. Ind. Electron.* **2014**, *61*, 5966–5973. [CrossRef]
33. Lipo, T. *Introduction to AC Machine Design*; IEEE Press Series on Power Engineering; Wiley: Hoboken, NJ, USA, 2017.
34. Williamson, S.; Muller, M.A. Calculation of the impedance of rotor cage end rings. *IEE Proc.-B* **1993**, *140*, 51. [CrossRef]
35. Wallmark, O.; Bitsi, K. Iron-Loss Computation Using Matlab and Comsol Multiphysics. In Proceedings of the 2020 International Conference on Electrical Machines (ICEM), Gothenburg, Sweden, 23–26 August 2020; Volume 1, pp. 916–920. [CrossRef]
36. Boglietti, A.; Cavagnino, A.; Ionel, D.M.; Popescu, M.; Staton, D.A.; Vaschetto, S. A General Model to Predict the Iron Losses in PWM Inverter-Fed Induction Motors. *IEEE Trans. Ind. Appl.* **2010**, *46*, 1882–1890. [CrossRef]
37. Krasopoulos, C.T.; Beniakar, M.E.; Kladas, A.G. Multicriteria PM Motor Design Based on ANFIS Evaluation of EV Driving Cycle Efficiency. *IEEE Trans. Transp. Electrif.* **2018**, *4*, 525–535. [CrossRef]
38. Ganev, E. Selecting the Best Electric Machines for Electrical Power-Generation Systems: High-performance solutions for aerospace More electric architectures. *IEEE Electrif. Mag.* **2014**, *2*, 13–22. [CrossRef]